CrossMark

ORIGINAL PAPER

Plasmonic enhancement of the upconversion luminescence in a Yb^{3+} and Ho^{3+} co-doped gold-ZnO nanocomposite for use in multimodal imaging

Sasidharanpillai S. Syamchand[1] · Ravindran S. Aparna[1] · George Sony[1]

Abstract The authors report on upconversion (UC) nanocrystals based on a gold-ZnO nanocomposite that enables HeLa cells to be characterizes via fluorescence imaging (FI), magnetic resonance imaging (MRI) and upconversion luminescence (UCL) imaging. The Yb^{3+} and Ho^{3+} doped gold-ZnO nanocomposite (Au-ZnO:Yb^{3+}/Ho^{3+}) was fabricated through a microwave-assisted route and possesses an irregular morphology. Inductively coupled plasma mass spectrometry (ICP-MS) shows the doping fractions of Yb^{3+} and Ho^{3+} to be 4.0% and 0.38% respectively. The nanocomposite shows UCL upon NIR irradiation at a wavelength of 980 nm. The emission spectrum has two main emission bands, one peaking at 544 nm (green emission), and the other at 658 nm (red emission). The red emission is stronger than the green emission, and the pump power dependence of upconversion intensity underpins a 2-photon UC process. The inherent down-conversion luminescence (DCL) of ZnO is preserved with enhanced intensity in the gold-ZnO nanocomposite. The plasmonic enhancement of both UCL and DCL can be clearly observed. Doping with Ho^{3+} renders paramagnetism to the nanocomposite, with a magnetization value of 18.91 emu·g^{-1}

at room temperature. The Au-ZnO:Yb^{3+}/Ho^{3+} nanocomposite exhibit a longitudinal relaxivity (r_1) of 0.12 s^{-1}·mM^{-1} and a transverse relaxivity (r_2) of 27.23 s^{-1}·mM^{-1}. Their substantial transverse relaxivity makes the nanocrystals most viable T2 MRI contrast agents. The cytotoxicity of nanocomposite was tested in HeLa cells by applying the MTT assay and by morphological studies. The nanocrystals are found to be biocompatible in up to50 μg·mL^{-1} concentration for an incubation time of 48 h. The nanocomposite is well taken up by HeLa cells. Its biocompatibility, UCL, DCL and its substantial magnetism make this nanocomposite as most viable nanoprobe for multimodal imaging.

Introduction

Multimodal imaging (MMI) offers synergistic advantages over any single imaging modality and thereby substantially improves the potential of non-invasive medical diagnosis [1, 2]. Smart combinations of nanomaterials with different functional properties like luminescence or magnetism enable the development of multifunctional nanomedical platforms for MMI [3, 4]. Several constraints such as different concentration requirements of contrast agents for diffent modalities, stability and biocompatibility hinder the advancement in the prospecting of nanoprobes for MMI. ZnO nanoparticles recognized as versatile biocompatible materials due to their superior chemical stability, low toxicity and sufficient dispersibility [5]. These favorable properties together with inherent luminescence enable the applicability of ZnO as a host

✉ George Sony
emailtosony@gmail.com

Sasidharanpillai S. Syamchand
syamchand.ss@gmail.com

Ravindran S. Aparna
rsaparnanair@gmail.com

[1] Department of Chemistry, University of Kerala, Kariavattom Campus, Trivandrum, Kerala 695 581, India

matrix for the development of multifunctional nanosystems for MMI. Functionalized ZnO nanocrystals have been synthesized by various methods and are explored in different biomedical applications including bioimaging [6–8].

Upconversion (UC) nanomaterials represent an adaptable class of fluorophores, which are based on a nonlinear optical phenomenon in which two or more low energy photons in the near-infrared (NIR) region converted into a high energy photon [9]. Biocompatible UC nanomaterials are highly preferred as nanoprobes for MMI owing to their favorable characteristic features like large anti-Stokes shifts, sharp emission bands, lack of auto-fluorescence from biological samples, low photodamage and high photostability [10–12]. Core-shell type biocompatible UC nanomaterials are successfully employed in the bioimaging of living cells [3]. The Lanthanide based UC nanostructures mainly comprised of an inorganic host matrix and lanthanide ion dopants. The host matrices and the dopants are pivotal factors that determine efficiency of UC emission. The lanthanide ion dopants, which are categorized as sensitizers and activators provide a luminescence centre and the host matrices supply a platform for energy transfer between the dopants [13, 14]. The host matrix should have low lattice phonon energies as well as chemical stability, since matrices with minimum phonon energies have maximum radiative emission possibility [15]. It has been observed that ZnO is having relatively low phonon energy of 437 cm^{-1} and is a favorable host matrix for UC process. Owing to the existence of ladder-like energy levels, trivalent Er, Tm and Ho are often selected as activators. Large absorption cross section and favorable energy levels renders Yb^{3+} as a common sensitizer to enhance UC emission [16]. Several reports are available on lanthanide doped ZnO based UC nanomaterials [17, 18]. The nanocomposite of ZnO with gold received great attention due to their excellent photocatalytic activity and enhanced performance in light harvesting devices [19, 20]. Gold-ZnO nanocomposites are prepared by several methods and the photocatalytic activity is widely investigated [21, 22]. However, the UC phenomenon in such composites is seldom explored. The presence of plasmons has remarkable influence in the emission properties of ZnO nanoparticles and in this study gold-ZnO composite is selected as the host matrix to develop UC nanomaterials. The lanthanide ions (Yb^{3+} and Ho^{3+}) are selected as dopants in gold-ZnO composite due to the strong paramagnetic behaviour of Ho^{3+}, which facilitate the adaptability of the system in developing contrast agents (CAs) for magnetic resonance imaging (MRI).

MRI is a versatile imaging modality to visualize the internal structure and soft tissue morphology of the body. It is privileged by limitless depth of penetration, high spatial resolution and unparalleled soft tissue contrast [23]. The

diagnostic value of MRI can be substantially improved by the administration of CAs. They can be categorized as positive (T1 contrast) or negative (T2 contrast) and commonly used CAs are either Gd-complexes (T1 contrast agents) or iron oxides (T2 contrast agents) [24]. These well-liked CAs are appropriate only at lower magnetic field strengths and it has been observed that the imaging performance in MRI increases with magnetic field strength. But the T1 relaxivity (positive contrast) decreases with increasing field strength and T2 relaxation becomes more efficient. In this stage, the T2 CAs based on Ho and Dy are noteworthy due to their remarkable performance under high field strengths [25]. Ho^{3+} being a heavy metal ion that can attenuate X-rays and this quality throws light into the prospecting of Ho based CAs for computer tomography (CT) imaging. But high concentration requirement of Ho^{3+} is a barrier, which limits this possibility and hence the focus is to explore the inherent magnetism in Ho^{3+} to develop T2 CAs for MRI.

In the present study, we report the development of an UC nanostructure based on gold-ZnO composite matrix, in which lanthanide ions(Yb^{3+} and Ho^{3+}) are doped (Au-ZnO:Yb^{3+}/Ho^{3+}). The present system can be explored for potential application in UC luminescence (UCL) imaging, MRI and fluorescence imaging (FI).

Materials and methods

Materials

Zinc acetate dihydrate (97%) Holmium chloride hexahydrate (99.9%) and ascorbic acid (99%) were purchased from Alfa Aesar (www.alfa.com). Ytterbium acetate tetrahydrate (99.9 %) was purchased from Sigma-Aldrich (www.sigmaaldrich.com). Oleic acid is obtained from Spectrum chemicals (www.spectrumchemicals.com). Oleyl amine and hydrogen tetrachloroaurate trihydrate were procured from Otto chemie (www.ottochemie.lookchem.com). Tri-sodium citrate dihydrate was purchased from MERCK (www.merck.com). All chemicals were used as received without further purification. Deionized water was used in the experiments throughout.

Microwave assisted synthesis of $Yb^{3+}$and Ho^{3+}co-doped ZnO nanoparticles

$Yb^{3+}$and Ho^{3+}co-doped ZnO nanoparticles were prepared through a microwave (MW) assisted route by adopting a reported procedure with adequate modification [26]. In a typical method, 440 mg of Zn(OAc)$_2$. 2H$_2$O (2 mmol) is dissolved in a mixture of 2 mL oleic acid and 8 mL oleyl amine. Dopants are then added to the system (3.8 mg HoCl$_3$. 6H$_2$O, 0.01 mmol and 42.2 mg Yb(OAc)$_3$. 4H$_2$O, 0.1 mmol). The reaction

mixture was then heated in a hot oil bath with stirring to 120 °C and the temperature was maintained for 1 h. The reaction mixture was immediately removed from the oil bath and microwaved under full power for 15 min, in a domestic microwave oven. Following the MW irradiation, the precipitate was separated from the liquid phase by centrifugation. It is then dried at overnight. No additional washing was performed. The capping agents are removed through thermal treatment by annealing the NPs in a muffle furnace at 400 °C for 2 h.

Synthesis of Yb^{3+} and Ho^{3+} co-doped Au- ZnO nanocomposite (Au-ZnO:Yb^{3+}/Ho^{3+})

The Yb^{3+} and Ho^{3+} co-doped ZnO nanoparticles (300 mg) were immersed into a mixture of 2 mL of 0.01 M sodium citrate (0.02 mmol), 2 mL of 0.01 M $HAuCl_4$ (0.02 mmol), 4 mL of 0.01 M ascorbic acid (0.04 mmol) and 20 mL of deionized water and subjected to magnetic stirring at room temperature for 3 h. The composite is separated by centrifugation and washed with deionized water followed by absolute ethanol and then dried in vacuum oven at 60 °C for 24 h. The procedure is repeated with same quantity of Yb^{3+} and Ho^{3+} co-doped ZnO nanoparticles and different concentrations of $HAuCl_4$ (0.005 mmol to 0.025 mmol), by keeping the molar ratio of sodium citrate, $HAuCl_4$ and ascorbic acid as 1: 1: 2.

Particle characterization

Powder X-ray diffraction (XRD) analysis is conducted to test the crystallinity of Au-ZnO:Yb^{3+}/Ho^{3+} nanocomposite. The instrument used is Bruker AXS D8 Advance X-ray powder diffractometer (www.bruker.com) and CuKα radiation (λ = 1.5406 Å) is selected as the source of X-ray. Energy dispersive X-ray spectrum (EDX) is used to analyze the material composition and the instrument used is JEOL Model JED-2300 spectrometer (www.jeol.com). Scanning electron microscopy (SEM) images of the nanocomposite were recorded by using JEOL Model JSM-6390 LV scanning electron microscope. High resolution transmission electron microscope (HR-TEM) images of the nanocomposite were taken with a FEI Tacna T30 (www.fei.com) transmission electron microscope. The instrument is operating at 300 kV of acceleration voltage. Jasco FP-750 spectrofluorometer (www.jascoinc.com) is used to record the room temperature photoluminescence (PL) spectra of all the samples. The UC spectra of the nanocomposite were recorded using FLS920P Edinburgh analytical instrument (www.edinst.com). The instrument is equipped with an external 980 nm diode laser as the excitation source. The room temperature magnetization (M-H curve) of the nanocomposite was measured by using a Lakeshore 7410 vibrating sample magnetometer (www.lakeshore.com). Fourier transform

infrared (FTIR) spectra of all the samples were recorded with a Shimadzu IR Prestige 21 spectrometer (www.shimadzu.com) and the scanning range is from 400 to 4000 cm^{-1}. Digital images were taken using a digital camera (Sony Cyber-shot DSC-W 800, www.sony.co.in).

Inductively coupled plasma mass spectrometry (ICP-MS) analysis

The doping concentrations of lanthanide ion dopants Yb^{3+} and Ho^{3+} in Au-ZnO:Yb^{3+}/Ho^{3+} nanocomposite were estimated by inductively coupled plasma mass spectrometry (ICP-MS). The instrument used for this analysis is Thermo Scientific ICAP Qc (www.thermofisher.com). Prior to the analysis, the instrument is externally calibrated by using standard certified multi element solution (MERCK, www.merck.com). During the analysis, the ion optics was tuned using Thermo scientific Tune-B ICAP-Q solution in standard mode as well as KED mode. The doped nanocomposite was MW digested (Anton Paar, Multiwave 3000) in ultrapure aquaregia prior to the analysis. The digested sample is duly diluted with Milli-Q water and analysis is conducted at an operating plasma power of 1550 W.

r_1 and r_2 relaxivity measurements

Longitudinal (T1) relaxation and transverse (T2) relaxation times of Au-ZnO:Yb^{3+}/Ho^{3+} nanocomposite were measured using Bruker Avans 500 MHz NMR spectrometer. The relaxation time measurements were carried out at 25 °C in spin echo method with time to echo (TE) = 9 ms. The applied magnetic field strength is 11.7 T. The T_1 and T_2 relaxation times were measured by using a series of five aqueous solutions of different concentrations (1, 0.5, 0.125, 0.0625 mM of Ho^{3+}). The solutions were prepared by dilution of the nanocomposite with triply distilled water. Inverse of the relaxation times (1/ T_1 and 1/T_2) were plotted against Ho^{3+} concentration and the relaxivities (r_1 and r_2) were computed from the slopes of the curves.

Cell culture and cytotoxicity assay

Human cervical cancer cells (HeLa) were used for testing the cytotoxicity of the nanocomposite. HeLa cells were procured from NCCS, Pune, India (www.nccs.res.in). The cells were allowed to grown in Dulbecco's Modified Eagle's Medium (DMEM) supplemented with 10% fetal bovine serum (FBS) 1% penicillin and streptomycin solution at 37 °C and 5% CO_2. The cells were sub-cultured at regular intervals (70–80% confluence) and the doubling time was 24 h. The effect of Au-ZnO:Yb^{3+}/Ho^{3+} nanocomposite on the viability of HeLa cells was estimated by 3-(4, 5-dimethylthiazol-2yl)-2, 5 diphenyl-tetrazolium bromide

(MTT) assay. The assay is based on the reduction of yellow MTT by mitochondrial succinate dehydrogenase to an insoluble purple colored formazan product. In a typical assay procedure, HeLa cells (1×10^4 cells per well) were seeded in 96-well micro-plate and allowed to attach by keeping in the CO_2 incubator at 37 °C under standard culture conditions for overnight. After that the medium containing unattached cells were removed by taking out the medium using a micropipette. Fresh medium containing different concentrations (10, 20, 30, 40 and 50 µg·mL^{-1}) of nanocomposite were added and incubated in the CO_2 incubator at 37 °C for different time intervals (4, 8, 12, 24 and 48 h). After incubation, the medium was removed and supplemented with fresh a medium (50 µL) containing MTT (5 mg·mL^{-1}) and kept inside CO_2 incubator for another 4 h. After removing the medium containing MTT, the formazan crystals produced were completely dissolved in dimethyl sulphoxide (DMSO) solvent and the absorbance was measured at 570 nm. The percentage of viability was calculated using the equation,

$$\%\text{viability} = \frac{\text{absorbance of treated cells}}{\text{absorbance of control cells}} \times 100.$$

Fluorescent microscopic studies on cellular uptake of Au-ZnO:Yb³⁺/Ho³⁺ nanocomposite

The cellular uptake of Au-ZnO:Yb³⁺/Ho³⁺ nanocomposite was studied in HeLa cells. 100 µL of cell suspension (1×10^3 cells) were seeded in 96-well black micro-plate and allowed to attach for overnight by keeping in CO_2 incubator under culture conditions of 37 °C and 5% CO_2. The unattached cells were removed by pipetting and a fresh medium containing nanocomposite (50 µg·mL^{-1}) was added to the wells and incubated for another 4 h in CO_2 incubator under same conditions. After that the medium was removed by pipetting and the plates were washed with phosphate-buffered saline (PBS) to remove the free nanocomposite. The cells were then observed under fluorescent microscope and the images were captured. The instrument used is a Live Cell Bioimager (BD pathway TM Bioimage System, BD Biosciences, www.bdbiosciences.com).

Results and discussion

Synthesis of Au-ZnO:Yb³⁺/Ho³⁺ nanocomposite

The nanocomposite is fabricated by a two step process. In the first step, Yb³⁺ and Ho³⁺ co- doped ZnO nanoparticles are prepared through a MW assisted synthesis, by following a reported method with necessary modifications [26]. The precursor, zinc acetate is subjected to decomposition under MW irradiation in a mixture of oleic acid and oleyl amine. It has been observed that the concentration of zinc acetate, ratio of oleic acid to oleyl amine and the MW irradiation time have substantial role in controlling the size and morphology of the ZnO nanoparticles. In the present synthesis, 0.2 M zinc acetate is used and an optimized volume ratio of 1: 4 (oleic acid to oleyl amine) is maintained for an irradiation time of 15 min. The lanthanide ion dopants (Yb³⁺ and Ho³⁺, in 1: 10 M ratio) are added to the reaction mixture prior to MW irradiation and it enabled their successful doping in the ZnO nanoparticles. The nanoparticles (ZnO:Yb³⁺/Ho³⁺) are then annealed to remove the capping agents and to improve crystallinity. In the second step, ZnO:Yb³⁺/Ho³⁺ nanoparticles are converted into Au-ZnO:Yb³⁺/Ho³⁺ nanocomposite by the incorporation of gold nanoparticles. The gold nanoparticles are prepared using the reagents HAuCl₄, sodium citrate, and ascorbic acid in an optimized molar ratio of 1: 1: 2. The total synthesis of Au-ZnO:Yb³⁺/Ho³⁺ nanocomposite is depicted in Scheme 1.

Characterization of Au-ZnO:Yb³⁺/Ho³⁺ nanocomposite

The crystallographic characteristics of the nanocomposite are invariably related to functional properties like luminescence and magnetism. The crystallinity of the Au-ZnO:Yb³⁺/Ho³⁺ nanocomposite was tested by the X-ray powder diffraction (XRD) analysis. The XRD pattern of the nanocomposite is shown in Fig. 1a. The spectrum revealed the co-existence of hexagonal phase ZnO with cubic phase Au in the composite.

The diffraction peaks are in good agreement with the data reported in JCPDS card no. 36–1451(wurtzite, *P63mc*) and 04–0784 (cubic phase Au, *Fm3m*). The XRD spectrum of ZnO:Yb³⁺/Ho³⁺ nanoparticles are given in electronic

Scheme 1 Schematic illustration of the total synthesis of Au-ZnO:Yb³⁺/Ho³⁺ nanocomposite
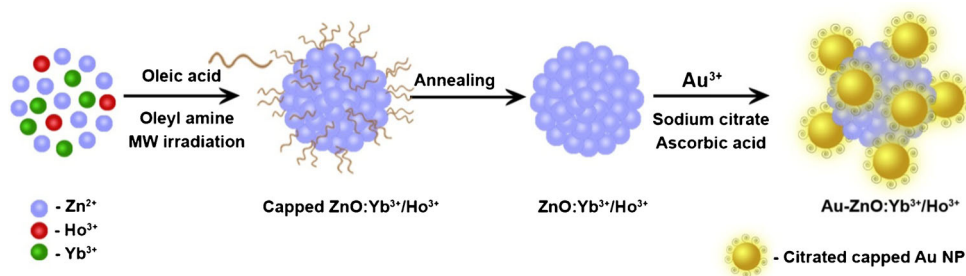
Fig. 1 a X- ray diffraction spectrum and (**b**) energy dispersive X-ray analysis spectrum of Au-ZnO:Yb^{3+}/Ho^{3+} nanocomposite
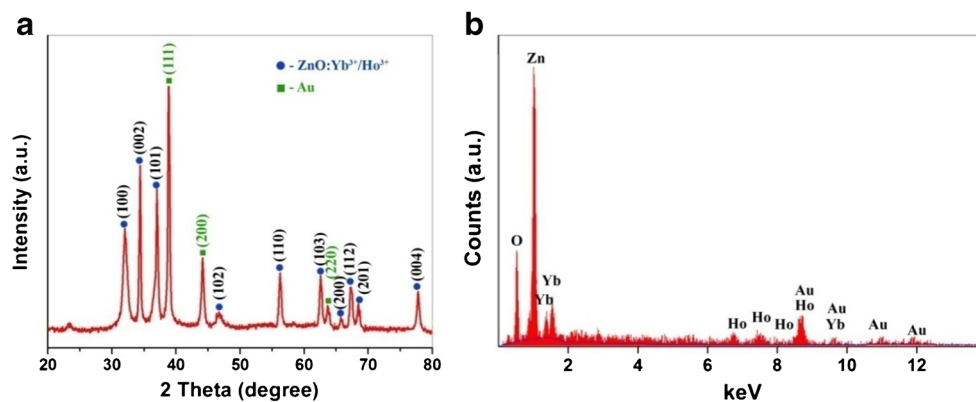

supplementary material (ESM, Fig. S1). The diffraction peaks can be indexed to ZnO with hexagonal wurtzite structure (JCPDS no.36–1451). The results indicated that the structure of ZnO nanoparticles was not changed after lanthanide ions (Yb^{3+} and Ho^{3+}) doping. This led to the conclusion that the lanthanide ions were efficiently doped into the ZnO matrix. The energy dispersive X-ray (EDX) analysis is performed to check the chemical purity and elemental compositions of the nanocomposite. The EDX spectrum of Au-ZnO:Yb^{3+}/Ho^{3+} nanocomposite is shown in Fig. 1b. The spectrum displays elemental peaks related to Zn, O, Au, Yb and Ho. The EDX spectrum of ZnO:Yb^{3+}/Ho^{3+} nanoparticles (Fig. S2, ESM) display all elemental peaks other than Au. The concentration of the lanthanide ion dopants in the nanocomposite were estimated by ICP-MS analysis and the results shown that 3.97% of Yb^{3+} and 0.38% of Ho^{3+} are present.

The digital images of ZnO:Yb^{3+}/Ho^{3+} nanoparticles and Au-ZnO:Yb^{3+}/Ho^{3+} nanocomposite (Fig. S3, ESM) revealed that the white color of ZnO nanoparticles changed to bluish black during the composite formation. This is attributed to the visible light absorption capability of gold-ZnO nanocomposite. From the FT-IR spectra of ZnO: Yb^{3+}/Ho^{3+} nanoparticles and the nanocomposite (Fig. S4, ESM) it can be inferred that practically no change occurs in the FT-IR pattern upon incorporation of Au into ZnO matrix, except the occurrence of additional peak at 1620 cm^{-1}. This peak is due to the stretching vibration of C = O group in citrate capped Au NPs. The intense peak around 500 cm^{-1} is due to Zn-O bond and the band at 1640 cm^{-1} corresponds to the bending vibrations of adsorbed water [27]. The morphology and size of Au-ZnO:Yb^{3+}/Ho^{3+} nanocomposite were analyzed by SEM and HR-TEM. The SEM image of ZnO:Yb^{3+}/Ho^{3+} nanoparticles (Fig. S5, ESM) showed the existence of nearly spherical nanoparticles. However, the SEM image of Au-ZnO:Yb^{3+}/Ho^{3+} nanocomposite (Fig. S6, ESM) depicted nanosized composite with irregular morphology, which implied the change in morphology associated with composite formation. The HR-TEM image of the composite (Fig. 2) agrees well with the SEM results and confirmed the existence of nanosized composite.

The HR-TEM clearly revealed the rough surface of the as-prepared nanocomposite and the spacing of the lattice fringes was found to be 0.23 nm.

Upconversion luminescence in Au-ZnO:Yb^{3+}/Ho^{3+} nanocomposite

The nanocomposite shows UC luminescence when excited by NIR photons of 980 nm (diode laser as the excitation source) and the UC emission spectra is shown in Fig. 3a. The two emission bands, peaking at 544 nm (green emission) and 658 nm (red emission) corresponds to ($^5F_4 + {}^5S_2$) $\rightarrow {}^5I_8$ and $^5F_5 \rightarrow {}^5I_8$ transitions of Ho^{3+}. The intensity of red emission is slightly higher than that of green emission. The UC emission intensity (I_{up}) is related to the exciting power (I_{ex}) as per the relation $I_{up} \propto (I_{ex})^n$ and here n represents the number of photons involved in the UC process.
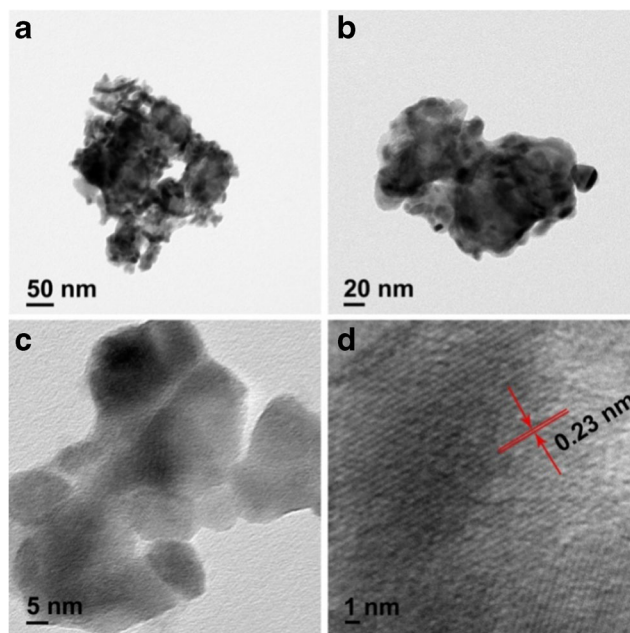
Fig. 2 HR-TEM images of Au-ZnO:Yb^{3+}/Ho^{3+} nanocomposite

a

b
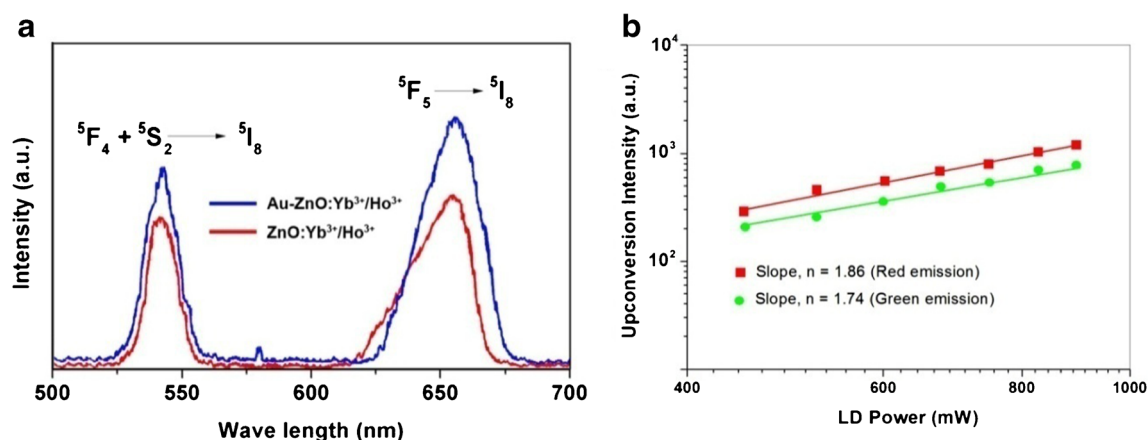
Fig. 3 **a** Upconversion emission spectra and (**b**) log-log plots of pump power dependence of the green and red emissions in Au-ZnO:Yb³⁺/Ho³⁺ nanocomposite

The pump power dependence of UC luminescence intensity is analyzed to find out n. The log-log plots of pump power dependence of the green and red emission is shown in Fig. 3b. The values of n (slope) for the red and green emissions were 1.86 and 1.74 respectively. These values of n support a 2-photon process, which mainly contributes to the red and green emissions. The mechanism of UC process in ZnO: Yb^{3+}/Ho^{3+} nanoparticles is well established and similar mechanism can be proposed for Au-ZnO:Yb^{3+}/Ho^{3+} nanocomposite [17]. Yb^{3+} ion serve as an effective sensitizer due to its large absorption cross section and high doping concentration (3.97%) compared to Ho^{3+} (0.38%). The energy levels of Ho^{3+} and Yb^{3+} ions together with possible UC mechanism are given in ESM (Fig. S7). The transitions in Ho^{3+} from excited states to $^5I_8$ ground level are responsible for green as well as red emission [17, 28].

From Fig. 3a it is clear that the emission intensity in Au-ZnO:Yb^{3+}/Ho^{3+} nanocomposite is greater than that in ZnO:Yb^{3+}/Ho^{3+} nanoparticles. This is due to the plasmonic enhancement in upconversion. It has been observed that localized surface plasmon resonance (LSPR) could enhance the fluorescence of an adjacent fluorophore which is placed at an appropriate distance from the metal nanostructures [29]. In the present study, the proximity of LSPR is explored to enhance UC luminescence in ZnO:Yb^{3+}/Ho^{3+} nanoparticles by attaching Au-plasmons through the Au-ZnO nanocomposite formation. Several mechanisms have been proposed to describe the effect of plasmons in UC luminescence and one reasonable mechanism considers the plasmonic structures as optical nanoantennas enabling improved reception and transmission of incident electromagnetic radiation by the upconverter [30]. The plasmonic antenna locally concentrates the incident field and enhances absorption, thereby improving the reception of the incident light by the upconverter. The plasmonic antenna can also enhance emission by increasing the radiative decay rate in the emitter. Thus, the existence of the plasmonic antenna enables the enhancement in UC

luminescence. However in certain cases, the plasmonic antenna quenches the UC emission by increasing the non radiative decay path. The quenching or enhancement depends on several factors such as spectral overlap between emission and absorption frequencies, polarization, pump power dependence and nature of the plasmonic antenna. These factors should be optimized and meticulously tuned to achieve desired enhancement or quenching. In the present system, the plasmonic enhancement in red region is greater than that of green region. This is probably due to the spectral overlap between the plasmonic absorption band and UC emission band in the green region.

Down-conversion luminescence

The down-conversion luminescence in Au-ZnO:Yb^{3+}/Ho^{3+} nanocomposite is due to the presence of luminescent ZnO quantum dots (QDs). The photoluminescence (PL) of ZnO consists of an exciton related ultraviolet (UV) emission and the defect related visible emission. The UV emission is considered as the characteristic emission of ZnO, and is due to the band edge transition or the exciton combination. The visible emission is associated with the intrinsic or extrinsic defects in ZnO. These defects mainly include oxygen vacancies, oxygen interstitials, zinc vacancies or zinc interstitials. The visible emission color can be tuned from blue to yellow [31, 32]. The presence of lanthanide ion dopants (Yb^{3+} and Ho^{3+}) has no detrimental effect in the luminescent properties of ZnO and hence ZnO:Yb^{3+}/Ho^{3+} nanoparticles are well luminescent. The PL spectra of ZnO:Yb^{3+}/Ho^{3+} nanoparticles and Au-ZnO:Yb^{3+}/Ho^{3+} composite with different Au concentrations are shown in Fig. 4.

From the spectra it is clear that the presence of Au has substantial effect in the luminescence of ZnO:Yb^{3+}/Ho^{3+} nanoparticles. The luminescence intensity keeps on increasing with Au^{3+} concentration up to an optimized concentration of 0.02 mmol of Au^{3+}, which is added during the synthesis of the nanocomposite. The increase in emission intensity is due to
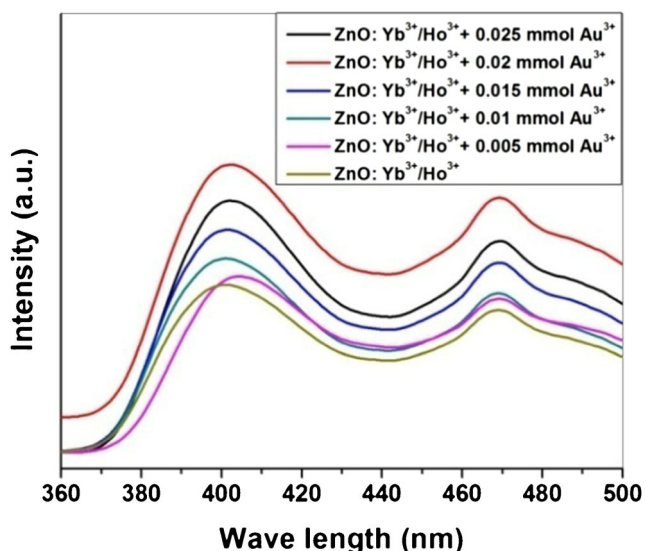
Fig. 4 The photoluminescence spectra of Au-ZnO:Yb^{3+}/Ho^{3+} nanocomposite

the enhancement of the surface plasmon resonance (SPR) induced local electric field on Au, which focuses the electromagnetic radiations (excitation beam) on to ZnO nanoparticles and accelerates the generation of electron-hole pairs. The recombination of conduction band electrons and valence band holes lead to more intense luminescence in the presence of Au. However, above certain level of Au concentration the electron-hole pairs show reluctance to recombination and it causes quenching. The luminescence quenched Au-ZnO system can perform as promising photoctalysts [27].

Magnetic property and relaxivities (r_1 and r_2)

Au-ZnO:Yb^{3+}/Ho^{3+} nanocomposite exhibit magnetism due to the presence of highly paramagnetic lanthanide ion dopant,
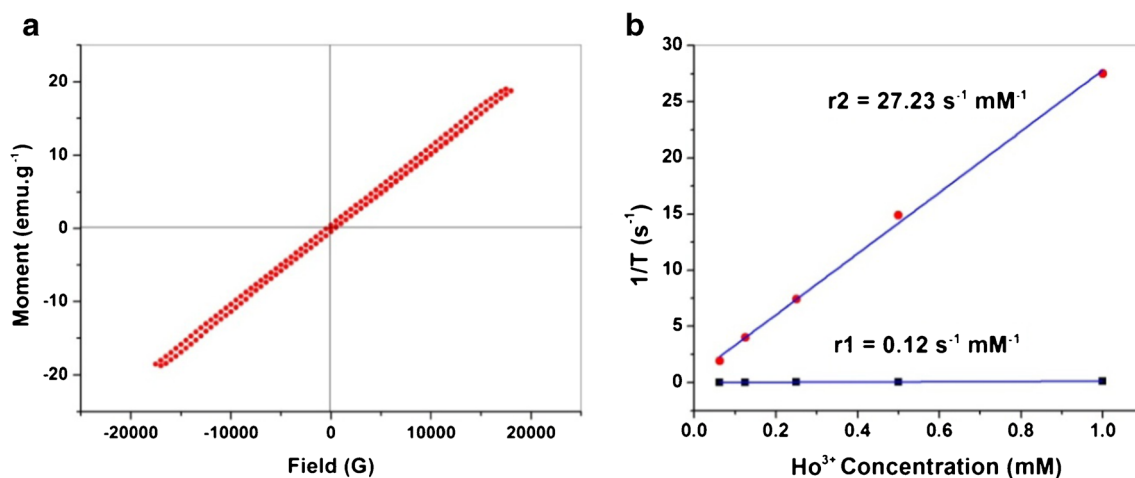
Ho^{3+}. The magnetic properties are studied by vibrating sample magnetometry (VSM) analysis and the room temperature magnetization against applied field (M-H) curve (Fig. 5a) clearly depicts the paramagnetic nature of the nanocomposite.

The magnetization value of the composite doped with 3.97% of Yb^{3+} and 0.38% of Ho^{3+} is observed as 18.91 emu·g^{-1}. It has been proposed that Dy^{3+} and Ho^{3+} can perform as efficient T2 contrast agents in intermediate and high magnetic field strengths, owing to their very short electronic relaxation time due to highly anisotropic ground state. Several reports on T2 contrast agents based on paramagnetic lanthanide ions such as Dy, Ho, Tb and Er are available in literature [33, 34]. One of the key factors which permit the adaptability of the nanocrystals as a contrast agent is the water proton relaxivity. The water proton relaxivity of the nanocomposite is measured to prove the applicability of the present system as a potential holmium based T2 MRI contrast agent. The longitudinal (T_1) and transverse (T_2) relaxation times of the nanocomposite are separately determined by using standard solutions of the nanocomposite with different concentrations (1, 0.5, 0.125, 0.0625 mM) of Ho^{3+}, with the aid of NMR instrument. The solutions of different concentrations are prepared from the nanocomposite which contains 0.38% of Ho^{3+}. The reciprocal of longitudinal and transverse relaxation times ($1/T_1$ and $1/T_2$) are calculated and plotted against Ho^{3+} concentration. The slopes of the curves (Fig. 5b) are evaluated to obtain longitudinal and transverse relaxivities. The present system shows a longitudinal relaxivity (r_1) 0.12 s^{-1}·mM^{-1} and transverse relaxivity (r_2) 27.23 s^{-1}·mM^{-1}. The high r_2 relaxivity invariably suggest the adaptability of the nanocomposite as holmium based T2 MRI contrast agent.

Cytotoxicity of Au-ZnO:Yb^{3+}/Ho^{3+} nanocomposite

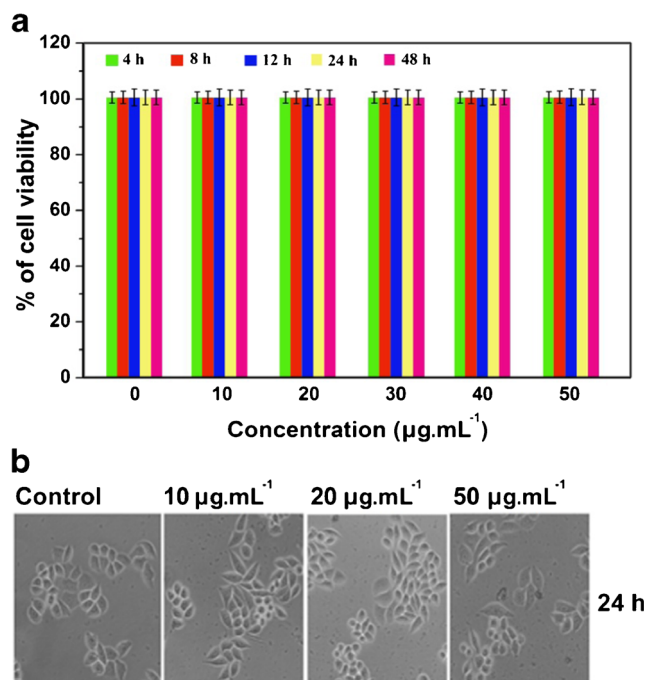The nanocomposite exhibits considerable degree of multifunctional properties like up and down-conversion luminescence

Fig. 5 a The room temperature magnetization against applied magnetic field (M-H) curve and (**b**) plots of $1/T_1$ and $1/T_2$ inverse relaxation times of Au-ZnO:Yb^{3+}/Ho^{3+} nanocomposite

a

b

Fig. 6 **a** MTT assay showing the non-toxicity of Au-ZnO:Yb^{3+}/Ho^{3+} nanocomposite in HeLa cells and (**b**) phase contrast microscopic images showing the effect of nanocomposite on cell morphology of HeLa cells

and magnetism, which strongly propose their applicability in multimodal imaging. The biocompatibility of the nanocomposite must be ensured prior to their application *in vivo*, since it is a major concern that limits the applicability in bioimaging. The cytotoxicity of Au-ZnO:Yb^{3+}/Ho^{3+} nanocomposite is tested by MTT assay in HeLa cells. The assay is performed with different concentrations of the nanocomposite at different incubation times and the results are shown in Fig. 6a.

The assay results confirmed the non-toxicity of nanocomposite up to concentration 50 µg·mL^{-1} for 48 h of incubation. As an additional evidence of biocompatibility, the effect of the nanocomposite on the morphology of the HeLa cells was tested through standard procedures at different concentrations (10, 20 and 50 µg·mL^{-1}) for an incubation period of 24 h.

The phase contrast microscopic images are shown in Fig. 6b and the results revealed that up to 50 µg·mL^{-1} concentration for 24 h of incubation, the morphology of the cells remains the same. The MTT assay and cell morphological analysis invariably proved that the synthesized nanocomposite is biocompatible and nontoxic to live cells.
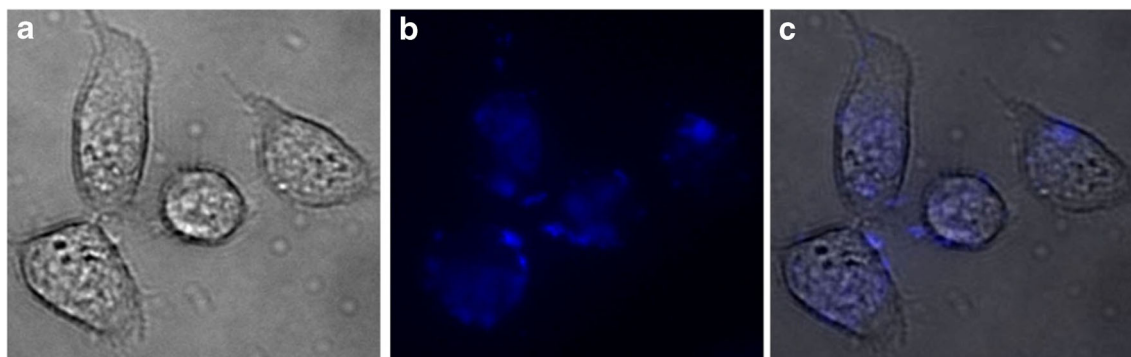
Cellular uptake of Au-ZnO:Yb^{3+}/Ho^{3+} nanocomposite

Bioimaging is a prevailing tool in biological research, since it offers a unique approach to visualize the morphological details of the cells. A wide variety of nanosized materials including UC nanomaterials are explored in fluorescent bioimaging [35]. The down-conversion luminescence in the nanocomposite can be explored in the fluorescent imaging of the cancer cells. The cellular uptake is a pre-requisite for the exploration of *in vivo* or *in vitro* fluorescent imaging capability of the nanocrystals. In this view point, the cellular uptake of the nanocomposite in HeLa cells were tested by incubating the nanocomposite for 4 h and the fluorescence is monitored by a fluorescence microscope. The images generated are shown in Fig. 7a, b and c.

From the results it is clear that the nanocomposite cross the cellular membrane and exhibit considerable degree of cellular uptake. Thus the present system can be explored for further receptor targeted fluorescent imaging of the cancer cells by conjugation with receptor targeting moieties like folic acid (FA).

Conclusion

In summary, we prepared lanthanide ions (Yb^{3+} and Ho^{3+}) doped gold-ZnO nanocomposite with luminomagnetic properties through a microwave assisted synthetic route. The said nanocomposite (Au-ZnO:Yb^{3+}/Ho^{3+}) exhibited UC luminescence as well as magnetism due to the presence of lanthanide ion dopants and down-conversion luminescence due to ZnO. The UC emission spectrum of the nanocomposite contains

Fig. 7 Fluorescent microscopic images showing the cellular uptake of Au-ZnO:Yb^{3+}/Ho^{3+} nanocomposite in HeLa cells: **a** phase contrast image (**b**) fluorescent image and (**c**) merged image

two bands centered at 544 nm (green emission) and 658 nm (red emission). The red emission is more intense and the 2-photon UC process is confirmed by the pump power dependence on UC emission intensity. Au-plasmons substantially enhance both up and down-conversion luminescence in the present system. Studies on magnetic properties confirmed paramagnetism of the nanocomposite, which is attributed to the presence of lanthanide ion, Ho^{3+}. The relaxivity measurements (r_1 and r_2) of the nanocomposite revealed a substantial r_2 relaxivity 27.23 $s^{-1} \cdot mM^{-1}$. The said nanocomposite was analyzed for toxicity through MTT assay and the effects of nanocrystals on the morphology of HeLa cells were tested. The results proved the biocompatibility of the composite. The cellular uptake of Au-ZnO:Yb^{3+}/Ho^{3+} nanocomposite is demonstrated in HeLa cells. As a future perspective, The UC and down-conversion luminescence can be explored in bioimaging and the substantial r_2 relaxivity can be utilized in developing Ho based T2 MR contrast agents. Thus, the up and down-conversion luminescence, favorable r_2 relaxivity and biocompatibility together make the present system adaptable for potential trimodal imaging.

References

1. Padmanabhan P, Kumar A, Kumar S, Chaudhary RK, Gulyás B (2016) Nanoparticles in practice for molecular-imaging applications: an overview. Acta Biomater 41:1–16
2. Lee SY, Jeon SI, Jung S, Chung IJ, Ahn C-H (2014) Targeted multimodal imaging modalities. Adv Drug Deliv Rev 76:60–78
3. Sun L, Liu T, Qiu Y, Liu J, Shi L, Wolfbeis OS (2014) Direct formation of mesoporous upconverting core-shell nanoparticles for bioimaging of living cells. Microchim Acta 181:775–781
4. Syamchand SS, Sony G (2015) Multifunctional hydroxyapatite nanoparticles for drug delivery and multimodal molecular imaging. Microchim Acta 182:1567–1589
5. Yin Q, Jin X, Yang G, Jiang C, Song Z, Sun G (2014) Biocompatible folate-modified Gd^{3+}/Yb^{3+}-doped ZnO nanoparticles for dualmodal MRI/CT imaging. RSC Adv 4:53561–53569
6. Xiong H-M (2013) ZnO Naoparticles applied to Bioimaging and drug delivery. Adv Mater 25:5329–5335
7. Zhu P, Weng Z, Li X, Liu X, Wu S, Yeung KWK, Wang X, Cui Z, Yang X, Chu PK (2016) Biomedical applications of functionalized ZnO nanomaterials: from biosensors to Bioimaging. Adv Mater Interfaces 3:1500494–1500523
8. Zhao B, Yao Y, Yang K, Rong P, Huang P, Sun K, An X, Li Z, Chen X, Li W (2014) Mercaptopropionic acid- capped Mn^{2+}:ZnSe/ZnO quantum dots with both downconversion and upconversion emission for bioimaging applications. Nano 6:12345–12349
9. Sun L-D, Wang Y-F, Yan C-H (2014) Paradigms and challenges for Bioapplication of rare earth Upconversion luminescent nanoparticles: small size and tunable emission/excitation spectra. Acc Chem Res 47:1001–1009
10. Mader HS, Kele P, Saleh SM, Wolfbeis OS (2010) Upconverting luminescent nanoparticles for use in bioconjugation and bioimaging. Curr Opin Chem Biol 14:582–596
11. DaCosta MV, Doughan S, Han Y, Krull UJ (2014) Lanthanide upconversion nanoparticles and applications in bioassays and bioimaging: a review. Anal Chim Acta 832:1–33
12. Yang Y (2014) Upconversion nanophosphors for use in bioimaging, therapy, drug delivery and bioassays. Microchim Acta 181:263–294
13. Dong H, Sun L-D, Yan C-H (2013) Basic understanding of the lanthanide related upconversion emissions. Nano 5:5703–5714
14. Chen C, Li C, Shi Z (2016) Current advances in lanthanide-doped Upconversion nanostructures for detection and Bioapplication. Adv Sci 1600029:1–26
15. Zhou J, Liu Q, Feng W, Sun Y, Li F (2015) Upconversion LuminescentMaterials: advances and applications. Chem Rev 115:395–465
16. Haase M, Schafer H (2011) Upconverting Naoparticles. Angew Chem Int Edn 50:5808–5829
17. Yu X, Liang S, Sun Z, Duan Y, Qin Y, Duan L, Xia H, Zhao P, Li D (2014) Microstructure and upconversion luminescence in Ho^{3+} and Yb^{3+} co-doped ZnO nanocrystalline powders. Opt Commun 313:90–93
18. Bai Y, Wang Y, Yang K, Zhang X, Song Y, Wang CH (2008) Enhanced upconverted photoluminescence in Er^{3+} and Yb^{3+} codoped ZnO nanocrystals with and without li^+ ions. Opt Commun 281:5448–5452
19. Li P, Wei Z, Wu T, Peng Q, Li Y (2011) Au-AnO hybrid Nanopyramids and their photocatalytic properties. J Am Chem Soc 133:5660–5663
20. Ho Y-C, Kao S-H, Lee H-C, Chang S-K, Lee C-C, Lin C-F (2015) Investigation of the localized surface plasmon effect from au nanoparticles in ZnO nanorods for enhancing the performance of polymer solar cells. Nano 7:776–783
21. Wang X, Kong X, Yu Y, Zhang H (2007) Synthesis and characterization of water-soluble and bifunctional ZnO-au nanocomposites. J Phys Chem C 111:3836–3841
22. Peralta MDLR, Pal U, Zeferino RS (2012) Photoluminescence (PL) quenching and enhanced photocatalytic activity of au-decorated ZnO Nanorods fabricated through microwave-assisted chemical synthesis. ACS Appl Mater Inter 4:4807–4816
23. James ML, Gambhir SS (2012) A molecular imaging primer: modalities, imaging agents, and applications. Physiol Rev 92:897–965
24. Nicolay K, Strijkers G, Grull H (2013) Gd- containing nanoparticles as MRI contrast agents In: Merbach A et al (ed) The chemistry of contrast agents in medical magnetic resonance imaging, 2nd edn, Wiley, UK, pp 449–483
25. Das GK, Johnson NJJ, Cramen J, Blasiak B, Latta P, Tomanek B, vanVeggel FCJM (2012) $NaDyF_4$ nanoparticles as T2 contrast agents for ultrahigh field magnetic resonance imaging. J Phys Chem Lett 3:524–529
26. Herring NP, AbouZeid K, Mohamed MB, Pinsk J, El-Shall MS (2011) Formation mechanisms of gold-zinc oxide hexagonal Nanopyramids by heterogeneous nucleation using microwave synthesis. Langmuir 27:15146–15154
27. Mondal C, Pal J, Ganguly M, Sinha AK, Jana J, Pal T (2014) A one pot synthesis of au-ZnO nanocomposites for plasmon-enhanced sunlight driven photocatalytic activity. New J Chem 38:2999–3005

28. Dong H, Du S-R, Zheng X-Y, Lyu G-M, Sun L-D, Li L-D, Zhang P-Z, Zhang C, Yan C-H (2015) Lanthanide nanoparticles: from design toward Bioimaging and therapy. Chem Rev 115:10725–10815

29. Chen G, Qiu H, Prasad PN, Chen X (2014) Upconversion nanoparticles: design, Nanochemistry, and applications in Theranostics. Chem Rev 114:5161–5214

30. Wu DM, García-Etxarri A, Salleo A, Dionne JA (2014) Plasmon-enhanced Upconversion. J Phys Chem Lett 5:4020–4031

31. Zhang Z-Y, Xiong H-M (2015) Photoluminescent ZnO nanoparticles and their biological applications. Materials 8:3101–3127

32. Zeng H, Duan G, Li Y, Yang S, Xu X, Cai W (2010) Blue luminescence of ZnO nanoparticles based on non-equilibrium processes: defect origins and mission controls. Adv Funct Mater 20:561–572

33. Norek M, Peters JA (2011) MRI contrast agents based on dysprosium or holmium. Progress in NMR 59:64–82

34. Kattel K, Park JY, Xu W, Kim HG, Lee EJ, Bony BA, Heo WC, Lee JJ, Jin S, Baeck JS, Chang Y, Kim TJ, Bae JE, Chae KS, Lee GH (2011) A facile synthesis, in vitro and in vivo MR studies of D-glucuronic acid-coated ultra small Ln_2O_3 (ln =Eu, Gd, Dy, ho, and Er) nanoparticles as a new potential MRI contrast agent. ACS Appl Mater Interfaces 3:3325–3334

35. Wolfbeis OS (2015) An overview of nanoparticles commonly used in fluorescent bioimaging. Chem Soc Rev 44:4743–4768